Electronic, Structural, and Magnetic Properties of Cobalt Aggregates Embedded in Polypyrrole

N. Watanabe,[†,‡] J. Morais,[§] S. B. B. Accione,[†] Â. Morrone,[§] J. E. Schmidt,[§] and M. C. Martins Alves*[,†,§]

Laboratório Nacional de Luz Síncrotron, P.O. Box 6192, 13084-971 Campinas, Brazil, Instituto de Química, UNICAMP, P.O. Box 6154, 13083-970 Campinas, Brazil, and Instituto de Física, Universidade Federal do Rio Grande do Sul, Avenida Bento Gonçalves, 9500, 91501-970 Porto Alegre, Brazil

Received: October 1, 2003; In Final Form: January 10, 2004

In this paper, we report on the synthesis and characterization of cobalt aggregates electrochemically incorporated on composite polypyrrole films. XAS (X-ray absorption spectroscopy) was used to probe the atomic local order in these composites and to furnish new insights into the metal/polymer interaction. A complete understanding of the incorporation process and its evolution was achieved by in situ XAS measurements at different stages of the electrochemical process. These results indicate that the reaction starts with the Co^{2+} entrapped in the polymeric matrix as a complex $[-[(C_4H_2N)_3CH_3(CH_2)_{11}OSO_3^-]_6Co^{2+}]$. The reduction of this complex leads to the synthesis of Co aggregates in the film. Measurements at the O and N K edges evidence that the main interaction between Co aggregates and the polymer is verified via Co−N bonds, the N originating from the polypyrrole (PPy) amine group. The pH effect on the metal/polymer interaction is discussed. Scanning electron microscopy (SEM) measurements show the formation of dendritic-like cobalt aggregates on the film surface. The magnetic response obtained by in situ alternating gradient field magnetometry (AGFM) allows prediction of the possibility of obtaining a magnetic polymer with superparamagnetic particles with sizes below 10 nm. Our results are the first steps toward the development of an advanced material with exciting potential for future recording media application.

Introduction

The confinement of nanoclusters in polymeric matrixes allows for the development of materials of technological and fundamental scientific relevance. One may predict potential applications in the fields of electrocatalysis,[1−5] biosensors,[6,7] microelectronics,[8,9] and magnetism.[10−12]

These composites can be produced by electrochemistry, which is an economic, versatile, and highly controllable method, ideally adapted to the engineering of nanostructured advanced materials. A large number of studies have focused on the development of sensors and catalysts, limiting the studies to the electrodeposition of Ag, Au, Pt, Cu, Pb, Pd, and Pt on polymers.[13] There are very few reports addressed to the fabrication of electrodeposited Co nanoclusters[14] embedded in a polymeric matrix. Tailoring the Co aggregates' properties for further applications in recording media is a synthetic challenge.

Magnetic properties are strongly dependent on the particle size as well as the crystalline structure and the chemical bonding at the surface.[15] So, it is of great importance to have the ability to obtain the electronic and structural characterization of the metal ion at different stages of the electrochemical process that leads to the formation of the Co nanoclusters. It is also important to characterize the interaction existent between the nanoclusters and the polymeric matrix because it may influence the final properties of the material.[16]

We report here, for the first time, an investigation of the incorporation of cobalt on polypyrrole (PPy) in the presence of a surfactant (sodium dodecylsulfate (SDS)). To accomplish the detailed characterization of the electronic and structural properties of these composite films, we took advantage of the X-ray absorption spectroscopy (XAS) technique that provides short-range order information on a selected atom in a matrix.[17] We used the same methodology applied in a previous study[18] based on Cu/PPy/DS (DS = dodecylsulfate anion).

In situ XAS measurements at the Co K edge were obtained in an electrochemical cell especially designed for this proposal. Ex situ measurements at the N and O K edges were performed to verify the influence of the metal on the electronic properties of the PPy/DS composite. The morphology of the cobalt aggregates was verified by SEM.

Finally, in situ magnetic measurements were obtained during the electrochemical growth of the Co/PPy/DS films, using in situ alternating gradient field magnetometry (AGFM).

Experimental Section

A. Sample Preparation. The cobalt/PPy/DS samples were electrochemically synthesized in an aqueous solution composed of 0.01 M $CoSO_4$ (Puratronic, 99.999%), 0.01 M $CH_3(CH_2)_{11}OSO_3^-Na^+$(SDS) (Mallinckrodt, 95%), 0.3 M H_3BO_3 (Synth, 95%), and 0.02 M pyrrole (Alfa Aesar, 98%, purified by distillation just before use) in Millipore Milli-Q deionized water. A working electrode of glassy carbon (Goodfellow, 99.99%) was polarized using a platinum-wire counter electrode, and its potential was measured vs an Ag/AgCl reference electrode. An EG&G PAR model 237A potentiostat was used to control the electrochemical conditions.

PPy films were obtained at +0.9 V (vs Ag/AgCl) during 200 s, producing films approximately 0.3 μm thick. The potential of 0.9 V was chosen, based on the pyrrole oxidation wave. The cobalt deposition was performed at three different potentials:

* To whom correspondence should be addressed. E-mail: mcalves@if.ufrgs.br.
[†] Laboratório Nacional de Luz Síncrotron.
[‡] UNICAMP.
[§] Universidade Federal do Rio Grande do Sul.

10.1021/jp036940y CCC: $27.50
Published on Web 03/09/2004

−0.6, − 0.8, and −1.2 V (vs Ag/AgCl), applied during 600 s in order to attain the equilibrium of the system. The XAS measurements were then performed.

B. X-ray Absorption Measurements. In situ XAS measurements at the cobalt K edge were performed at the Laboratório Nacional de Luz Síncrotron (LNLS), using the XAS beam line.[19] A "channel-cut" Si (111) crystal monochromatized the collimated X-ray beam. Vertical slits of 0.4 mm placed before the monochromator provided an energy resolution of 2.0 eV. The monochromator was calibrated at the Co K edge using a Co metal foil.

A thin-layer electrochemical cell, developed at LNLS, was mounted on a goniometer stage, and the measurements were performed with the incident beam at 10° with respect to the substrate surface. The measurements were acquired in fluorescence mode, using a NaI scintillator. This detector was placed on the top of the electrochemical cell.

Co K edge XANES spectra were recorded from 8900 to 9160 eV with 0.8 eV steps and 2 seconds per point (s/pt). EXAFS spectra were recorded from 8900 to 9500 eV with a 2.0 eV step and an acquisition time of 2 s/pt. An average of five acquisitions was performed to improve the signal-to-noise ratio. XANES measurements at the O and N K edges were performed at the SGM (spherical grating monochromator) beam line at LNLS. The resolving power ($E/\Delta E$) of the spherical grating is better than 3000. The spectra were collected in the total electron-yield mode by measuring the sample current. The spectra were normalized to the photon flux using the yield of a gold mesh, 95% transparent, placed 15 cm upstream from the sample. Photon beam dimensions were about 1 mm × 1 mm at the sample, and normal incidence was used.

C. XAS Data Analysis. The WINXAS program[20] was used for data analysis. A linear preedge background was subtracted, and the spectra were normalized to the height of the absorption edge. The EXAFS signal between 2.5 and 10.4 $Å^{-1}$ was Fourier-transformed with a k^3 weighting and a Kaiser window. Structural parameters were obtained from least-squares fitting in the k space using experimental phase shift and amplitude extracted from $CoSO_4$ and Co metal. We also used theoretical phase shifts and amplitudes deduced from the FEFF code.[21] In the fitting procedure, the number of free parameters did not exceed the number of independent data points given by the Nyquist theorem.[22]

D. Scanning Electron Microscopy. The morphology of the films was observed using a JSM-6330F field emission scanning microscope at 5 kV. Since the samples were conductive, no further metallic film deposition was required.

E. AGFM Measurements. Magnetic measurements were recorded at room temperature using a homemade in situ AGFM.[23] The PPy/DS film was deposited on a substrate of gold polycrystalline thin film, evaporated on mica with a surface area of 6 mm^2. The polymer was deposited at 0.90 V during 200 s, and the film thickness was approximately 0.2 μm. The cobalt electroreduction was performed at −1.20 V during 200 s, yielding 6.14 μg of elemental Co. During the deposition process, the parallel component of the magnetization was probed as a function of time. Hysteresis loops were recorded just after the metal electrodeposition, so the potential was then settled to −0.10 V, where no further deposition or dissolution occurs, and the hysteresis loops were acquired. In these measurements, the field was applied in the plane of the film. The diamagnetic contribution originating from the sample holder was measured independently and subtracted from the hysteresis curve in the data-analysis procedure.

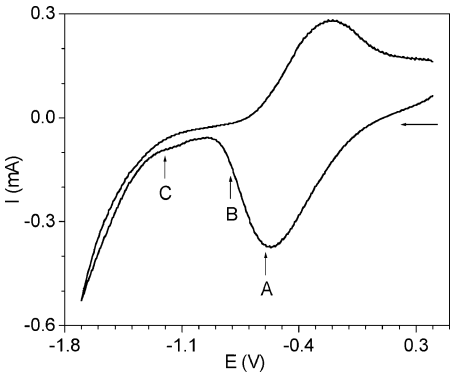

Figure 1. Cyclic voltammetry of PPy/DS film deposited on glassy carbon immersed in 0.01 M $CoSO_4$−0.3 M H_3BO_3. The sweep rate was 20 mV/s. Arrows indicate the potentials at which the XAS spectra were acquired: A, −0.60 V; B, −0.80 V; and C, −1.20 V.

Results

A. Electrochemistry. The electrochemical response of the PPy/DS film deposited on glassy carbon in the presence of Co^{2+} ions enables the definition of potentials of interest for the subsequent XAS measurements. The cyclic voltammogram (Figure 1) displays a reduction peak around −0.6 V, followed by an abrupt increase of the current from −1.0 V, caused by hydrogen evolution. An oxidation peak is observed at −0.20 V in the reverse scan.

B. XANES at the Co K Edge. The position of the X-ray absorption-edge jump for a given element is dependent on its oxidation state. The near-edge features (XANES) are dependent on the symmetry of the local environment. The comparison of the obtained XANES spectra with appropriate standard compounds allows the determination of electronic and structural properties of the cobalt incorporated in the films.

The Co K edge XANES spectra were acquired at −0.60, −0.80, and −1.20 V and compared to references of an aqueous solution of $CoSO_4$ and Co metal **(**Figure 2A). The spectrum of the Co^{2+} ions in solution shows a small preedge peak (feature 1, 1s → nd transition) and a very intense absorption edge[24] (feature 2, 1s → 4p transition), characteristic of Co^{2+} ions in an octahedral geometry. Structures 3 and 4 are attributed to multiple scattering effects.[25] The Co metal spectrum presents a strong preedge (feature 1′, 1s → p−d hybridized state[25]) and multiple scattering features characteristic of Co in a hexagonal compact (HCP) packing (structures 2′, 3′, and 4′).

At −0.60 V, the XANES spectrum is similar to that of the aqueous solution of $CoSO_4$. At −0.80 V, there is a strong decrease of the absorption-edge height with concomitant development of the characteristic oscillations of metallic cobalt (features 2′, 3′, and 4′). At −1.20 V, the spectrum is identical to that of metallic cobalt.

The comparison of the spectrum obtained at −0.60 V with that of Co^{2+} ions in solution (Figure 2B) evidences some relevant differences. At −0.60 V, a wider absorption edge (feature 2) is observed, which may be associated with higher disorder around cobalt. In addition, features 3 and 4 and the minimum around 7750 eV (see the arrows) are shifted to higher energy. These results indicate that the Co^{2+} ions at −0.60 V are not in solution but bonded to the polymeric matrix.

The Fourier transform (FT) of the EXAFS signal (Figure 3) reflects the average radial distribution function around Co atoms. At −0.60 V, the peak around 1.3 Å is related to Co−O and/or Co−N distances. The large width and the low amplitude in the FT peak at this potential evidence the existence of high structural disorder. At −0.80 V, there is a small contribution of the light

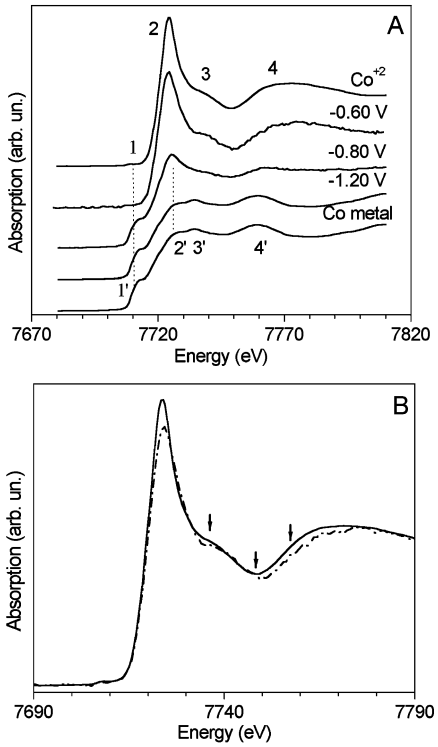

Figure 2. (A) In situ Co K edge XANES spectra acquired at −0.60, −0.80, and −1.20 V in comparison with the spectra of an aqueous solution of $CoSO_4$ and Co metal references. (B) Comparison of the spectra obtained for the aqueous solution of 0.01 M $CoSO_4$, (full line) and at −0.60 V (dash dot line).

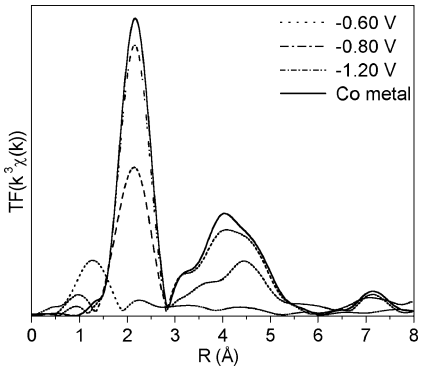

Figure 3. Fourier transforms of the EXAFS data.

TABLE 1: Results Obtained from the Quantitative Analysis of the Coordination Shell Yielding the Coordination Number (*N*), Distance (*R*), and the Debye−Waller Factor (σ)

	N	pair	*R* (Å)	σ^2 (Å^2)
-0.60 V	6 ± 0.5	(Co−O/N)	2.12 ± 0.05	0.0368 ± 0.0074
-0.80 V	3.5 ± 0.5	(Co−O/N)	1.99 ± 0.01	−0.0032 ± 0.0010
	5.0 ± 0.5	(Co−Co)	2.50 ± 0.01	0.0030 ± 0.0006
-1.20 V	12.0 ± 0.5	(Co−Co)	2.50 ± 0.01	0.0176 ± 0.0004
$CoSO_4$	6	(Co−O)	2.06	
Co metal	12	(Co−O)	2.50	0.0055

elements (O/N) and Co−Co distances show up. At this potential, one observes distances characteristic of next-nearest neighbors (distances higher than 3 Å), indicating medium-range order of the atomic shells. Finally, at −1.20 V, there are only Co−Co distances.

The quantitative analysis of the first shell (Table 1) shows that, at −0.60 V, the cobalt atoms are surrounded by 6 ± 0.5 atoms located at 2.12 ± 0.05 Å. The large Debye−Waller factor (σ^2) value (0.0368 ± 0.0074) points to a highly disordered structure.

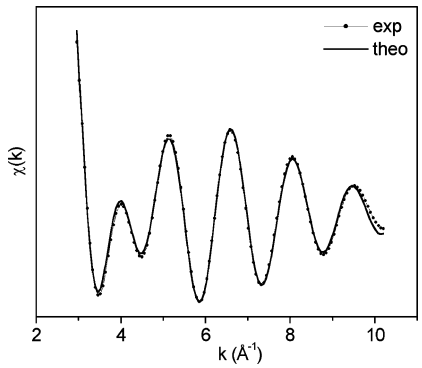

Figure 4. Two shell fittings obtained for the spectrum acquired at −0.80 V.

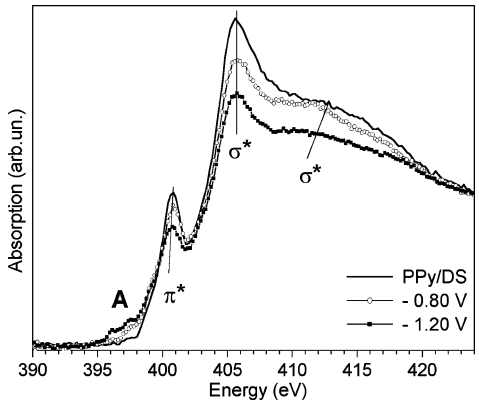

Figure 5. N K edge XANES spectra for the PPy/DS films acquired at −0.80 and −1.20 V in comparison with a pure PPy/DS film.

At −0.80 V, two distances of $R = 1.99 \pm 0.01$ and 2.50 ± 0.01 Å show the coexistence of cobalt in the oxidized and reduced (Co^0) forms. The Co−Co distance corresponds to that of bulk cobalt. The quality of the fit can be observed in Figure 4.

At −1.20 V, the obtained values of $N = 12 \pm 0.5$ and $R = 2.56 \pm 0.01$ Å suggest the complete reduction of metallic cobalt in the majority of the film. The higher value of the Debye−Waller factor (0.0176 ± 0.0004) in comparison to that found for metallic cobalt (0.0055) suggests higher disorder in the first shell.

C. XAS at N and O K Edges. The XANES measurements at the N and O K edges were performed to verify eventual changes in the polymer heteroatoms, induced by the presence of the Co metal. So, we have compared the PPy/DS films obtained at −0.8 and −1.20 V to a pure PPy/DS film.

The N K edge spectrum (Figure 5) of the PPy/DS film displays a first electronic transition at about 402 eV related to an N 1s → 2pπ* dipole transition. The two high-energy resonances that appear at about 405 and 413 eV are the delocalized σ* resonances (N 1s → σ*(2p)) that are referred to in transition from the N 1s level to the delocalized σ* C−N molecular orbital.[26] The σ* excitations are intramolecular resonance effects localized around the central atom and involve long-range effects.[27]

In Figure 5, one observes a gradual decrease of the π* transition with a concomitant arising of a lower energy transition of about 397 eV (structure A) going from the film prepared at −0.8 and −1.20 V. This new transition (structure A) may be associated with a new unoccupied state.

The O K edge features (Figure 6) are related to transitions from the O 1s level to states with some O np character.[28] The preedge peak (∼539 eV) is the π* resonance (O 1s → 2pπ*)

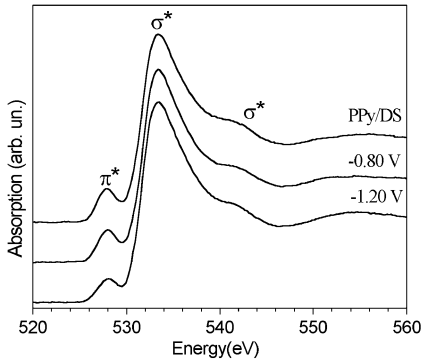

Figure 6. O K edge XANES spectra for the PPy/DS films obtained at −0.80 and −1.20 V in comparison with a pure PPy/DS film.

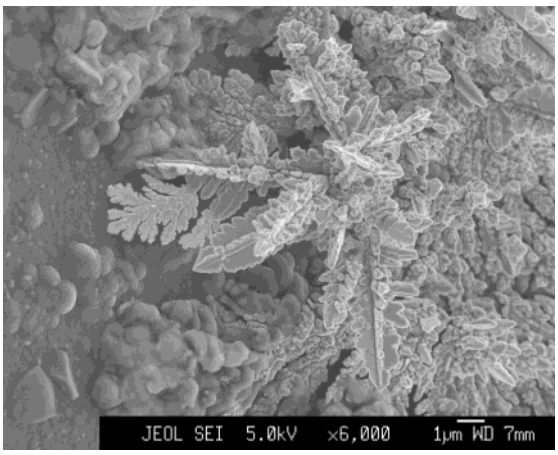

Figure 7. SEM image taken for the PPy/DS film obtained at −1.20 V.

and the broader structures (532−547 eV) are σ^* resonances. The spectra of the PPy/DS composite and the ones obtained at −0.8 and −1.20 V are practically identical.

D. SEM Measurements. SEM measurements allow characterization of the morphology of the Co aggregates entrapped on the film (Figure 7), obtained at −1.2 V. The image shows the corrugated structure of the polymeric film on the left and dendritic-like cobalt aggregates on the polymer surface. The size of the dendrites is dependent on the deposition time of cobalt.

E. AGFM Measurements. The potential pulses and the corresponding parallel component of the magnetization as a function of the time are presented in Figure 8A. The full line corresponds to the potential values assumed during the process. The polymer deposition is started at $t = 0$ s by stepping up the potential from the equilibrium and keeping it at 0.9 V. For 200 s, only the polymer is deposited and the cobalt deposition is then started by reducing the potential from +0.9 to −1.2 V. The magnetization curve (open circles) (0 s < t < 200 s) initially displays slightly negative slope that corresponds to the expected diamagnetic response from the polymer.[29] Once the cobalt incorporation starts (t > 200 s), the magnetization signal increases with the cobalt content.

The hysteresis loop was recorded just after the incorporation of Co during 200 s and setting the potential at −0.1 V, where no further incorporation or dissolution reaction occurs. The hysteresis loop is displayed in Figure 8B. From this measurement, it is possible to extract parameters such as the Mr/Ms ratio (Mr is the remanence and Ms is the saturation magnetization). In this case, the remanence is measured for the external field $H = 0$ and Ms is estimated at $H = 4346$ Oe. The Mr/Ms value corresponds to the squareness of the curve and assumes

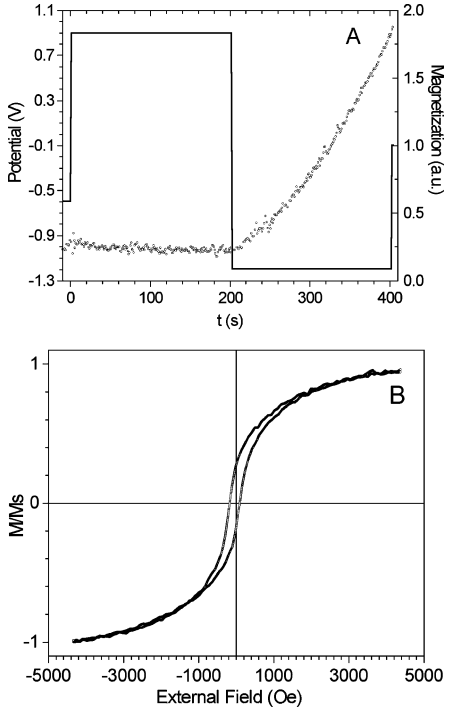

Figure 8. (A) Potential pulses (full line) and the corresponding parallel component of the magnetization (open circles) as a function of the deposition time. (B) Magnetization vs applied field plot for PPy/DS/Co film.

the value of 1 for a ferromagnetic system and 0 when superparamagnetic islands are present. For cobalt, the superparamagnetic regime is attained for particles with sizes below 6.7 nm.[29] From the hysteresis loop, the Mr/Ms ratio is about 0.24, and it is possible to deconvolute this curve in superparamagnetic and ferromagnetic contributions. The superparamagnetic component contributes to the rounded shape of the curve as well as to the decrease of the value for Mr/Ms. The coercive field value (H_c), measured when the magnetization or Mr/Ms = 0, is about 130 Oe. This value is coherent with others found in the literature for thin films.[22]

Discussion and Conclusion

The combination of the Co K edge XANES and EXAFS results allow us to affirm that the initial step of the electrochemical process, at −0.60 V, corresponds to the electroreduction of the PPy/DS film with concomitant uptake of Co^{2+} ions from the solution. The Co^{2+} ions assume an octahedral geometry in the polymeric network, with six (6 ± 1) neighbors at 2.12 ± 0.05 Å. The Debye−Waller factor (0.0368 ± 0.0074) obtained is much higher than the one found for the Cu/PPy/DS system[18] (0.0013 ± 0.00026). This value suggests the formation of a much-disordered system for Co composites. These results indicate that the reaction starts with the Co^{2+} entrapped in the polymeric matrix as a complex $[-[(C_4H_2N)_3CH_3(CH_2)_{11}OSO_3^-]_6\text{-}Co^{2+}]$. It is known that the electrochemical synthesis of polypyrrole involves three pyrrole units per counterion.[30]

At more reductive potentials, −1.20 V, the Co^{2+} ions from the solution are discharged, forming metallic cobalt (Co^0) on the polymeric matrix. At a less reductive potential, −0.80 V, a mixture of oxidized and reduced forms of Co are present. The complete reduction of the Co species entrapped in the film is achieved at −1.2 V. In fact, the SEM image shows that the cobalt aggregates assume dendritic shape with high surface area.

The O K edge XANES measurements demonstrated that O atoms are not disturbed by the presence of the cobalt aggregates.

Nevertheless, at the N K edge, a new transition was observed (structure A) that may be associated to a new unoccupied state. This result evidences that the cobalt aggregates induce changes in the electronic structure of the N from the PPy amine group and it is possible to associate the existence of an interaction between the metal to the PPy amine group. When heterocycles are in contact with a metal, a charge transfer to the metal occurs resulting in strong bonding. The interaction with the metal substrate leads to an important decrease of the π^* resonance.[31] The shift in the absorption threshold (structure A) might be associated with transitions to states in the band gap that have been emptied by charge transfer to the metal.[32]

In ref 18, we have indicated that the copper insertion into PPy/DS films occurs by means of Cu−O bonding instead of a Cu−N bond. The main difference between these two systems is the solution's pH. The Cu/PPy/DS films were synthesized at low pH, pH = 1.4, and, at this condition, the pyrrolic nitrogen is protonated, thus avoiding any interaction at the nitrogen linkages. In the case of the Co insertion, the synthesis condition has pH = 5.7. At that pH, the nitrogen of pyrrole is not protonated, allowing the nitrogen to interact with the cobalt, forming a Co−N bonding.

The magnetic hysteresis loop measured allows the prediction that interesting properties may be achieved in Co/PPy/DS systems. The Mr/Ms ratio obtained is consistent with the fact that ferromagnetic and superparamagnetic particles are present. It means that the size distribution is not very homogeneous. However, the superparamagnetic behavior comes from particles with sizes below 6.7 nm. Calculations concerning the estimation of the particle sizes and corresponding volumes are under way.

In conclusion, we have characterized the electronic and structural properties of Co aggregates in PPy/DS films deposited on glassy carbon. In situ XAS measurements at the Co K edge allowed us to follow the changes in the local structure during the electrochemical process at different stages. XAS measurements at the N and O K edges allowed us to ascertain that only the N displays modifications in its electronic structure after the metal deposition. This result suggests the existence of a Co−N interaction.

Regarding the nature of metal/polymer interaction, extensive discussions and divergences are currently presented in the literature. The major differences in the results are mainly caused by differences in the synthesis conditions, especially in the pH of the solution. This work has reported a powerful way to conclusively identify the changes in the electronic and structural properties in the different steps of the electrochemical synthesis.

The results concerning the magnetic response of the Co/PPy/DS films encourage future improvements in the synthesis conditions that will enable tailoring exclusive magnetic polymers for advanced applications.

Acknowledgment. We thank Miguel Abbate and Oswaldo Luiz Alves for fruitful discussions and suggestions. We are indebted to the staff of LNLS for operating the storage ring and the assistance during the experiments at the XAS and SGM beam lines. The beam time was supported by LNLS under the proposals XAS 656/00 and SGM 689/00 and 1064/02. Thanks are also addressed to Daniel Ugarte and Paulo C. Silva for their help during the SEM measurements. This work was partially supported by the Brazilian Funding agencies FAPESP (Project Nos. 99/07872-4, 97/06967-6, and 95/ 06439-4), Pronex, and FAPERGS. N.W. thanks the CNPq (Proc. No. 144894/98-0) for her Ph.D. fellowship.

References and Notes

(1) Crooks, R. M.; Lemon, B. I.; Sun, L.; Yeung, L. K.; Zhao, M. Q. *Top. Curr. Chem.* **2001**, *212*, 81.

(2) Cai, L. T.; Chen, H. Y. *Sens. Actuators, B* **1999**, *55*, 14.

(3) (a) Tourillon, G.; Garnier, F. *J. Phys. Chem.* **1984**, *88*, 5281. (b) Hepel, M. *J. Electrochem. Soc.* **1998**, *145*, 124. (c) Hepel, M.; Chen, Y. M.; Stephenson, R. *J. Electrochem. Soc.* **1996**, *142*, 498.

(4) Deronzier, A.; Moutet, J.-C. *Coord. Chem. Rev.* **1996**, *147*, 339.

(5) Tourillon, G.; Dartyge, E.; Fontaine, A.; Jucha, A. *Phys. Rev. Lett.* **1986**, *57*, 603.

(6) Mailley, P. *Talanta* **2001**, *55*, 1005.

(7) Kim, K. J.; Shahinpoor, M. *Polymer* **2002**, *43*, 797.

(8) Sershen, S. R.; Westcott, S. L.; Halas, N. J.; West, J. L. *Appl. Phys. Lett.* **2002**, *80*, 4609.

(9) White, H. S.; Kittlesen, G. P.; Wrighton, M. S. *J. Am. Chem. Soc.* **1984**, *106*, 5375.

(10) Khaibullin, R. I.; Zhikharev, V. A.; Osin, Y. N.; Zheglov, E. P.; Khaibullin, I. B.; Rameev, B. Z.; Aktas, B. *Nucl. Instrum. Methods Phys. Res., Sect. B* **2000**, *166*, 897.

(11) Langlais, V.; Arrii, S.; Pontonnier, L.; Tourillon, G. *Scr. Mater.* **2001**, *44*, 1315.

(12) Chen, J. P.; Sorensen, C. M.; Klabunde, K. J.; Hadjipanayis, G. C. *Phys. Rev. B* **1995**, *51*, 11527.

(13) (a) Chou, S.-H.; Rau, J.-R.; Chen, S.-C. *Electrochim. Acta* **1997**, *42* (15), 2313. (b) El-Giar, E. M.; Said, R. A.; Bridges, G. E.; Thomson, D. J. *J. Electrochem. Soc.* **2000**, *147* (2), 586. (c) Jovic, V. D.; Trisovic, T.; Jovic, B. M.; Vojnovic, M. *J. Electroanal. Chem.* **1996**, *408*, 149. (d) Hatchett, D. W.; Josowicz, J.; Janata, J.; Baer, D. R. *Chem. Mater.* **1999**, *11*, 289. (e) Rau, J.-R.; Chen, S.-C.; Tang, H.-Y. *Synth. Met.* **1997**, *90*, 115. (f) Cioffi, N.; Torsi, L.; Losito, I.; Di Franco, C.; De Bari, I.; Chiavarone, L.; Scamarcio, G.; Tsakova, V.; Sabbatini, L.; Zambonin, P. G. *J. Mater. Chem.* **2001**, *11*, 1434. (g) Hepel, M.; Dentrone, L. *Electroanalysis* **1996**, *8*, 996.

(14) Bello, M. E.; Pereira, E. C. *Mol. Cryst. Liq. Cryst.* **2002**, *374*, 107.

(15) Osuna, J.; deCaro, D.; Amiens, C.; Chaudret, B.; Snoeck, E.; Respaud, M.; Broto, J. M.; Fert, A. *J. Phys. Chem.* **1996**, *100*, 14571.

(16) Van Leeuwen, D. A.; Van Ruitenbeek, J. M.; de Jong, L. J.; Ceriotti, A.; Pacchioni, G.; Harberlen, O. D.; Rosch, N. *Phys. Rev. Lett.* **1994**, *73*, 1432.

(17) Koningsberger, D. C.; Prins, R. X-ray Absorption: Principles, Applications and Techniques of EXAFS, SEXAFS and XANES. In *Chemical Analysis*; John Wiley & Sons: New York, 1988; Vol. 92.

(18) Watanabe, N.; Morais, J.; Alves, M. C. M. *J. Phys. Chem. B* **2002**, *106*, 11102.

(19) Tolentino, H.; Ramos; A. Y.; Alves, M. C. M.; Barrea, R. A.; Tamura, E.; Cezar, J. C.; Watanabe, N. *J. Synchrotron Rad.* **2001**, *8*, 1040.

(20) Ressler, T. *J. Phys. IV* **1997**, *7*, C2-269.

(21) Rehr, J. J.; Mustre de Leon, J.; Zabinsky, S. I.; Albers, R. C. *J. Am. Chem. Soc.* **1991**, *113*, 5135.

(22) Lytle, F. W.; Sayers, D. E.; Stern, E. A. *Physica B* **1989**, *158* (1−3), 701.

(23) Gündel, A.; Cagnon, L.; Gomes, C.; Morrone, A.; Schmidt, J. *Phys. Chem. Chem. Phys.* **2001**, *3*, 3330.

(24) Briois, V.; Cartier, C.; Momenteau, M.; Maillard, P.; Zarembovich, J.; Dartyge, E.; Fontaine, A.; Tourillon, G.; Thuery, P.; Verdaguer, M. *J. Chim. Phys. Biol.* **1989**, *86* (7−8), 1623.

(25) Rehr, J. J.; Albers, R. C.; Zabinsky, S. I. *Phys. Rev. Lett.* **1992**, *69* (23), 3394.

(26) Henning, C.; Hallmeier, K. H.; Szargan, R. *Synth. Met.* **1998**, *92*, 161.

(27) (a) Henning, C.; Hallmeier, K. H.; Bach, A.; Bender, S.; Franke, R.; Hormes, J.; Szargan, R. *Spectrochim. Acta, Part A* **1996**, *52*, 1079. (b) Pavlychev, A. A.; Hallmeier, K. K.; Henning, C.; Szargan, R. *Chem. Phys.* **1995**, *201*, 547.

(28) Pedio, M.; Fuggle, J. C.; Somers, J.; Umbach, E.; Haase, J.; Lindner, Th.; Hofer, U.; Grioni, M.; de Groot, F. M. F.; Hillert, B.; Becker, L.; Robinson, A. *Phys. Rev. B* **1989**, *40*, 7924.

(29) (a) Cullity, B. D. *Introduction to Magnetic Materials*; Addison-Wesley Publishing: Menlo Park, CA, 1972. (b) Bozorth, R. M. *Ferromagnetism*; D. Van Nostrand Co.: Toronto, Canada, 1959; Vol. 2.

(30) Wood, G. A.; Irosh, J. O. *Synth. Met.* **1996**, *80*, 73.

(31) (a) Skotheim, T. A.; Yang, X. Q.; Chen, J.; Hale, P. D.; Inagaki, T.; Samuelson, L.; Tripathy, S.; Hong, K.; Rubner, M. F.; den Boer, M. L.; Okamoto, Y. *Synth. Met.* **1989**, *28*, C229. (b) Tourillon, G.; Raaen, S.; Skotheim, T. A.; Sagurton, M.; Garret, R.; Williams, G. P. *Surf. Sci.* **1987**, *184*, L345. (c) Stevens, P. A.; Upton, T. H.; Stöhr, J.; Madix, R. J. *Phys. Rev. Lett.* **1991**, *67* (12), 1653.

(32) Ritsko J. J. *Phys. Rev. Lett.* **1981**, *46* (13), 849.